C. R. Mecanique 341 (2013) 289–297

Contents lists available at SciVerse ScienceDirect

Comptes Rendus Mecanique

www.sciencedirect.com

Active control of the flow behind a two-dimensional bluff body in ground proximity

Sébastien Chaligné [a,b,*], Thomas Castelain [a,c], Marc Michard [a], Daniel Juvé [a]

[a] LMFA, UMR CNRS 5509, École centrale de Lyon, 36, avenue Guy-de-Collongue, 69134 Écully Cedex, France
[b] Volvo Group Truck Technology, Renault Trucks SAS, Cab Engineering Lyon, 99, route de Lyon, 69806 Saint-Priest Cedex, France
[c] Université Lyon 1, 43 Boulevard du 11 Novembre 1918, 69622 Villeurbanne Cedex, France

ARTICLE INFO

Article history:
Received 20 July 2012
Accepted after revision 31 October 2012
Available online 26 January 2013

Keywords:
Fluid mechanics
Flow control
Unsteady wake flow
Particle image velocimetry

ABSTRACT

Active flow control around a two-dimensional geometry positioned near the ground is experimentally studied. Results for two model configurations are reported: one square-back and the other with a flap added at the rear-corner. The model rear end static pressure and the near-wake flow properties are derived from wall-pressure measurements, high-speed Particle Image Velocimetry acquisitions and hot-wire anemometry. The control flow is obtained from a pulsed jet system driven in open loop. The study aims at distinguishing the individual influence of the passive flap and the control system. The actuation frequency is shown to be a determining parameter regarding rear end pressure increase.

1. Introduction

The objective of the present contribution is to demonstrate the effects of flow control on a two-dimensional bluff body, studied experimentally, and to find the relationship between the surface static pressure at the rear end of the model and the main characteristics of the wake flow.

Wake characteristics behind a two-dimensional bluff body depend on numerous parameters such as the Reynolds number, the characteristics of the incoming boundary layer developing on the body and the possible proximity of a wall. For instance, Shi et al. [1] investigate experimentally the influence of the ratio G/L for a cylinder with a square section of sides L positioned at a distance G from the ground. A decrease of this ratio allows mitigating, or even suppressing, the periodic vortex shedding phenomenon. Thus, the flow behind the body consists of an area of separated flow presenting a degree of intermittences depending on the ratio G/L. Aerodynamic forces such as lift and drag are strongly dependent on this parameter.

Aerodynamic drag reduction can be achieved by the use of different passive or active flow control solutions. Typical passive solutions, such as flaps or a boat tail positioned at the rear end, usually allow reducing the aerodynamic drag by vectoring the mean flow, thus narrowing the wake size. Both experimental [2,3] and numerical [4] studies taking into account ground effects show significant drag reduction using flaps or a boat tail. However, the efficiency of such solutions remains limited by the low flap inclination needed for the mean flow to stay attached.

Regarding active solutions, numerous studies as in [5,6] show that pulsed or synthetic jets positioned near the natural separation line allow delaying or suppressing the flow separation phenomenon. These two different types of fluidic actuators differ by their average mass flow, the pulsed jet having a positive net mass flow and the synthetic jet a zero net mass flow. Considering the interaction between an actuator coupled with a rectangular nozzle and a boundary layer developing on

* Corresponding author at: LMFA, UMR CNRS 5509, École centrale de Lyon, 36, avenue Guy-de-Collongue, 69134 Écully Cedex, France.
E-mail addresses: sebastien.chaligne@ec-lyon.fr (S. Chaligné), thomas.castelain@ec-lyon.fr (T. Castelain), marc.michard@ec-lyon.fr (M. Michard), daniel.juve@ec-lyon.fr (D. Juvé).

1631-0721/$ – see front matter
http://dx.doi.org/10.1016/j.crme.2012.10.043

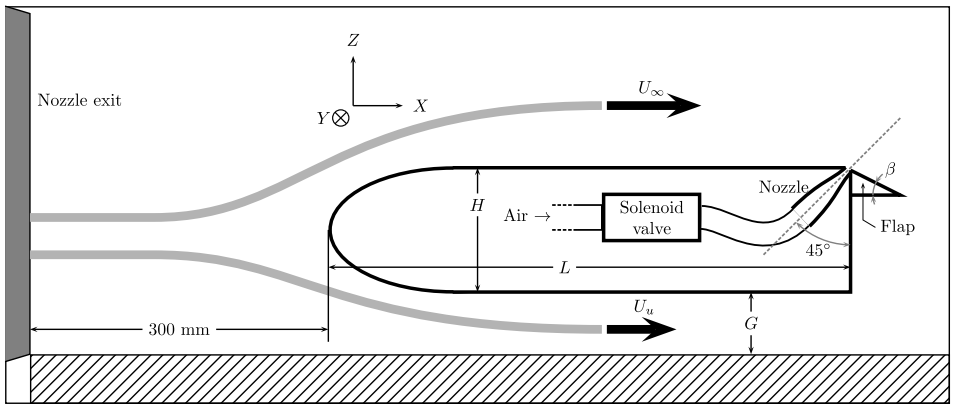

Fig. 1. Sketch of the experimental set-up. The model is represented here in the flap configuration; the square-back configuration is similar, the flap excepted.

a two-dimensional cylinder [7] or a ramp [8], the blowing phase of the jet generates a vortex structure leading to a local pressure decrease forcing the flow to reattach to the wall downstream of the natural flow separation line. In the specific case of synthetic jets, this effect is even stronger due to the suction phase occurring consecutively to the generation of the vortex structure. Hence, this forced reattachment induces a mean deflection of flow streamlines in direction of the wall downstream of the jet slot.

The effects of synthetic jets on detached flows are studied by Chun et al. [9] and Hasan [10] for a backward-facing step and Dandois et al. [8] for a two-dimensional ramp. These authors show that actuating a synthetic jet within a certain frequency range leads to a reduction of recirculation length, due to an increase in the intensity of velocity fluctuations within the shear layer issued from the flow separation. This frequency range is interpreted in these references as a signature of the existence of a convective flow instability.

Most studies involving pulsed or synthetic jets applied to simplified square-back geometries do not take the ground effect into consideration. Pastoor et al. [11] and Krajnovic et al. [12] study the wake flow mechanisms resulting from synthetic jets applied to a two-dimensional square-back geometry. Without ground proximity, they show that the use of synthetic jets at the rear end edges of the model allows forcing symmetric vortex shedding and thus delaying the wake instabilities. In this case, an increase of 40% of base pressure is obtained. El-Alti et al. [13] show numerically that combining flaps with synthetic jets can even further increase the base pressure.

Krentel et al. [14] investigate experimentally the influence of a pulsed jet system on the recirculation area behind a three-dimensional square-back model close to a floor and obtain a drag reduction of only 2.2%. Wassen et al. [15] perform numerical simulations on the same geometry and obtain a similar drag reduction with close to zero net power savings.

The aim of this experimental investigation is to study how a pulsed jet system combined with a passive flap modifies the aerodynamic drag acting on a two-dimensional square-back bluff body in ground proximity, this drag being mainly due to pressure losses at the geometry rear end. Two different model configurations are tested: a square-back configuration and a flap configuration. These two configurations allow estimating the individual influence of the passive flap and of the active flow control system on the static pressure at the model rear end.

2. Experimental setup

Experiments are conducted in an open test section wind tunnel. The flow comes out of a nozzle with an exit square section of 500×500 mm^2. The free stream velocity U_∞ is set to 25 m/s and constantly monitored by using a Pitot tube.

The model used is a two-dimensional bluff body represented in Fig. 1, which illustrates a side view of the test set-up. This model is positioned at a distance of 300 mm from the nozzle. Its length L, height H and width W are respectively 555 mm, 100 mm and 380 mm, resulting in a Reynolds number of $Re_H \approx 176\,000$.

The ground clearance G is set to 4 mm (i.e. $G/H = 4\%$) in order to take the ground proximity effect into account and to reduce the underside flow velocity U_u. This height ratio results in a velocity ratio U_u/U_∞ of 0.6. Two lateral transparent plates are positioned on each side of the model to ensure two-dimensional flow properties in the central part of the latter, where pressure and velocity measurements are performed. These properties are confirmed in the central upper part of the model by comparing the velocity profiles at different locations in the Y direction, 5 mm upstream the rear edge. In the configuration without flap, the velocity profiles compare well over at least 60% of the model width, the reference profile being that measured in the median plane. In this plane, the associated momentum thickness θ is 4.6 mm.

In this study, the flap angle and length are chosen as $\beta = 20°$ and $l = 50$ mm. The control flow is generated by a pulsed jet system, consisting of seven rapid solenoid valves coupled with a row of seven circular-to-rectangular section nozzles. Each nozzle exit section corresponds to a rectangular slot of thickness e = 0.3 mm and spanwise length $w = 50$ mm. Slots are positioned at the upper rear edge of the model and are oriented so that the jet angle with respect to the free stream flow direction is equal to 45°, as illustrated in Fig. 1. The spacing between two adjacent slots is 3 mm. The solenoid valves

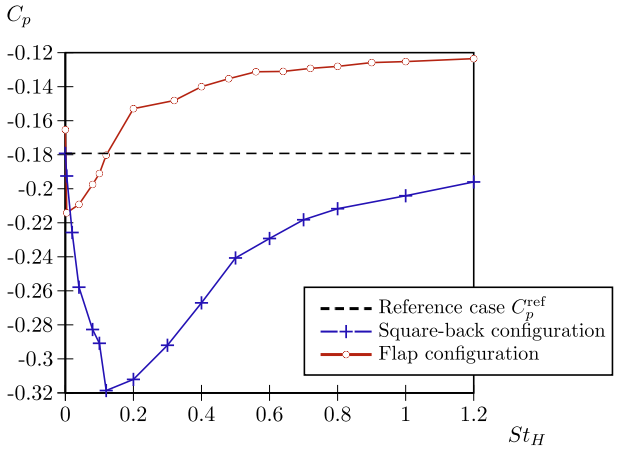

Fig. 2. Mean static pressure coefficient measured at the rear end of the model function of the actuation Strouhal number St_H for the square-back and flap configurations. $St_H = 0$ corresponds to the cases where pulsed jet system is off.

are driven in open loop and in phase by a Matrix HSDB900 Speed-Up card whose command signal is of square wave type with an actuation frequency F and a duty cycle of 50%.

Wall pressure measurements are carried out at the rear end of the model. Fifteen wall pressure taps are distributed along the median plane, each being connected to a Scanivalve system coupled with a Furness 0–200 mm H_2O manometer. Time-averaged values over two seconds are collected and the average of these values provides an estimate of the mean pressure p at the model rear end. Particle Image Velocimetry measurements are performed in the near-wake median plane using a Quantronix Laser (Darwin Duo Nd:YLF Dual Oscillator) and a high speed Phantom V12 camera. Sets of 2500 image couples are recorded at a rate of 3125 Hz. The dimensions of the field-of-view are $L_X/H = 2.15$ horizontally and $L_Z/H = 1.34$ vertically. The magnification factor of the optical setup corresponds to 0.16 mm/px. Recorded images are processed under DaVis using interrogation window sizes from 64×64 to 16×16 px^2 and an overlap of 50%.

In what follows, results are presented using four non-dimensional parameters. First, the usual definition of the momentum coefficient C_μ is used with the flow control parameter U_j being the jet velocity averaged over an actuation period, s the total area of the seven jet slots and S the frontal area of the model.

$$C_\mu = \frac{sU_j^2}{SU_\infty^2}$$

In the present work, C_μ is set at a constant value of 0.06% whatever the actuation frequency F. The corresponding value of U_j has been determined by a hot-wire anemometry study performed at the nozzle exit in quiescent conditions. The influence of the actuation frequency F on C_p is presented in terms of Strouhal numbers St_H based on U_∞ and H or St_θ involving θ.

$$St_H = \frac{FH}{U_\infty}; \qquad St_\theta = \frac{F\theta}{U_\infty}$$

Regarding pressure measurements, the mean static pressure coefficient is defined as below with ρ the air density and p_0 the free stream static pressure:

$$C_p = \frac{p - p_0}{\frac{1}{2}\rho(U_\infty)^2}$$

It is of interest here to distinguish the effects of the flap itself and the effects of the flap together with pulsed jets. In the following, the reference case corresponds to the square-back geometry without flap and with the pulsed jet system off.

3. Results

3.1. Mean static pressure measurements

The evolution of the mean static pressure coefficient C_p with the actuation Strouhal number St_H is given in Fig. 2. Results are provided for two configurations: the square-back configuration and the flap configuration. The value of $C_p^{ref} = -0.178$ obtained for the square-back configuration with the pulsed jet system off is considered as the reference value. The black dashed line in Fig. 2 is a reminder of C_p^{ref} and allows a quick estimate of the pressure gains associated with the use of the flow control system.

Regarding the square-back configuration, C_p is minimum when actuating at $St_H = 0.12$, which corresponds to $St_\theta = 0.0055$; this large decrease in C_p with respect to C_p^{ref} is linked to changes in the wake flow characteristics, as will be described in Section 3.2. In particular, the recirculation length is thought to be substantially modified, although no attempt was made to measure it in the present work. Referring to [9], a large decrease in the recirculation length is obtained for $St_\theta \approx 0.01$, in the case of a confined backward-facing step flow with a Reynolds number of a few tens of thousands. Nevertheless, despite the differences between the two set-ups, the values of St_θ leading to the minimum of the studied quantities are found to be of the same order of magnitude. Moreover, the evolution of C_p with the actuation frequency compares well to that of the recirculation length given in Fig. 3 of [9].

In any case for the square-back configuration, as shown in Fig. 2, no matter the actuation frequency for the pulsed jets, C_p remains always lower than C_p^{ref}. Therefore, the pulsed jet system by itself does not provide any reduction in pressure drag.

Considering now the flap configuration, the addition of the flap corresponds to a slight pressure recovery leading to a value of C_p equal to -0.164 with the pulsed jet system off. When the pulsed jet system is on, the evolution of C_p with St_H consists, as observed for the square-back configuration, in a decrease followed by an increase which begins at a lower frequency than that of the square-back configuration. With respect to this configuration, the drag penalty is weaker and occurs over a narrower St_H range. For higher St_H, C_p keeps increasing and seems to reach an asymptotic value leading to a significant drag reduction.

3.2. Time-averaged properties of the near-wake flow

For cases selected on the basis of C_p results, PIV measurements have been carried out. In the following, results obtained with square-back and flap configurations either with or without pulsed jet actuation are compared. The selected values of St_H are 0.1, representative of the St_H range in which the drag penalty is obtained and 1.2, for which the maximum value of C_p with control is reached. For each configuration, snapshots of the velocity magnitude field obtained by PIV in the near-wake region are depicted in Fig. 3. For the cases where the pulsed jet system is on, these snapshots are representative of what occurs periodically in the near-wake region.

Streamlines computed from the corresponding mean velocity fields are superimposed to these velocity maps and indicate the occurrence of flow vectoring due to the control system.

The flow around the model in the reference configuration illustrated in Fig. 3(a) presents some similarities with that around a backward-facing step [9,10] in spite of the presence of the lower shear layer coming from the underside. No alternating vortex shedding is observed because of ground proximity [1] and both shear layers will interact only considerably further downstream.

For $St_H = 0.1$, the vortex structure resulting from the incoming flow and pulsed jet interaction moves convectively and is amplified until reaching a size equivalent to the height of the model H, as seen in Fig. 3(c). Therefore, this large scale vortex structure induces a very low pressure area close to the model rear end. The interaction between this vortex structure and the lower shear layer makes the wake region even more unsteady.

For higher frequencies, large scale vortex structures are not observed. The structure induced by the incoming flow and pulsed jet interaction is convected and dissipated downstream of the slot as shown in Fig. 3(e). Interaction between both shear layers is weaker making the mean upper shear layer take a direction more horizontal than without actuation.

Regarding the flap configuration, the same unsteady phenomena as those described for the square-back occur. The influence of the actuation Strouhal number St_H on the interaction between the pulsed jet and the wake region stays similar in both cases which is coherent with the static pressure evolution with St_H depicted in Section 3.1. The main difference with the square-back configuration is the mean flow vectoring illustrated in Fig. 3 by plotting streamlines. Without the pulsed jet (Fig. 3(b)), the flow is detached from the flap wall and the mean streamlines are similar to those observed in Fig. 3(a). When the pulsed jet system is on, the control-induced vortex structures force the flow to be attached along the flap wall, thus vectoring the upper shear layer and reducing the wake size. This phenomenon is even more pronounced for the case actuated at $St_H = 1.2$ in Fig. 3(f).

Maps of the 2D kinetic energy of velocity fluctuations E_T are given in Fig. 4, where E_T is defined as:

$$E_T = \frac{1}{2}\left(u_{\text{rms}}^2 + v_{\text{rms}}^2\right)$$

For cases without actuation, as indicated in Figs. 4(a) and 4(b), the kinetic energy is essentially confined within the upper shear layer. For comparison, the maps of the kinetic energy when actuating at Strouhal number $St_H = 0.1$ are given in Figs. 4(c) and 4(d). The maximum of E_T in the wake is increased with respect to the cases without actuation. Moreover, a high level of energy is observed over the whole model height. This is consistent with the large scale structures observed in Figs. 3(c) and 3(d) and the interaction between both shear layers. For an actuation Strouhal number St_H of 1.2, as indicated in Figs. 4(e) and 4(f), the kinetic energy is lower in the flap configuration. Furthermore, the velocity fluctuations remain concentrated within the upper shear layer. These maps give support to the instantaneous velocity fields presented in Fig. 3 in highlighting the energy content of the large coherent structures induced by the control actuated at $St_H = 0.1$.

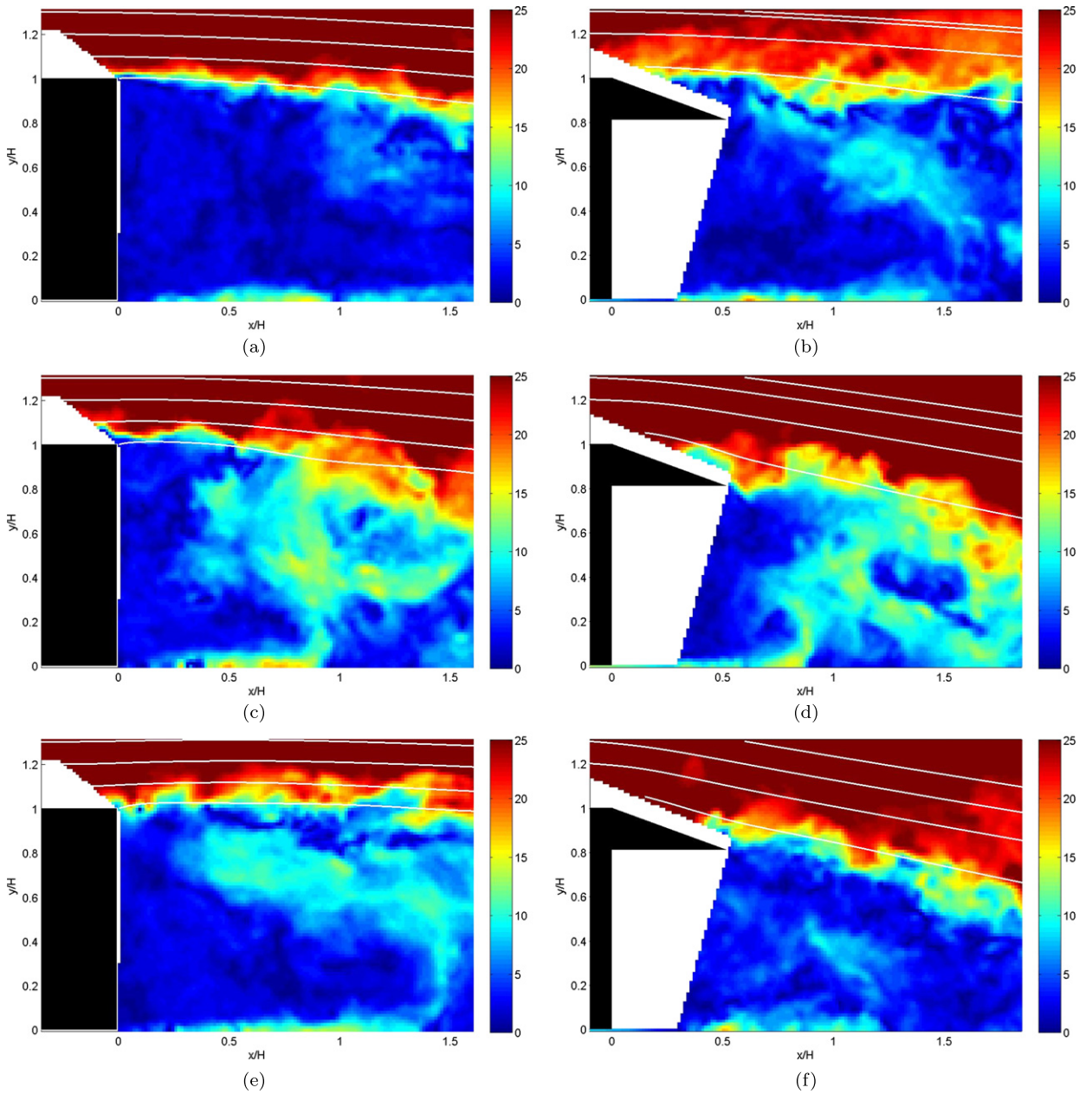

Fig. 3. Instantaneous velocity magnitude fields measured by PIV with in white streamlines of the mean flow:
• The square-back configuration with the pulsed jet system off (a), actuated at $St_H = 0.1$ (c) and $St_H = 1.2$ (e);
• The flap configuration with the pulsed jet system off (b), actuated at $St_H = 0.1$ (d) and $St_H = 1.2$ (f).
The origin of the coordinate system is taken at the lower edge of the model rear end.

3.3. *Characteristics of the coherent structures induced by the control*

To get a better understanding of the interactions between the incoming flow and the pulsed jet, the spatial and temporal coherence of the generated vortex structures is studied. The space–time correlation coefficient of vertical velocity fluctuations v, defined by (1), is computed for two points separated by $\vec{r}$ in space and a time delay τ.

$$R_{vv} = \frac{\langle v(\vec{x},t)v(\vec{x}+\vec{r},t+\tau)\rangle}{\langle v^2(\vec{x},t)\rangle} \tag{1}$$

In the following, one reference point is set fixed at a specified position $\vec{x}$ near the nozzle slot exit. Maps of R_{vv} are computed over the entire field obtained by PIV by varying the parameter $\vec{r}$. The reference position $\vec{x}$ is illustrated in Fig. 5

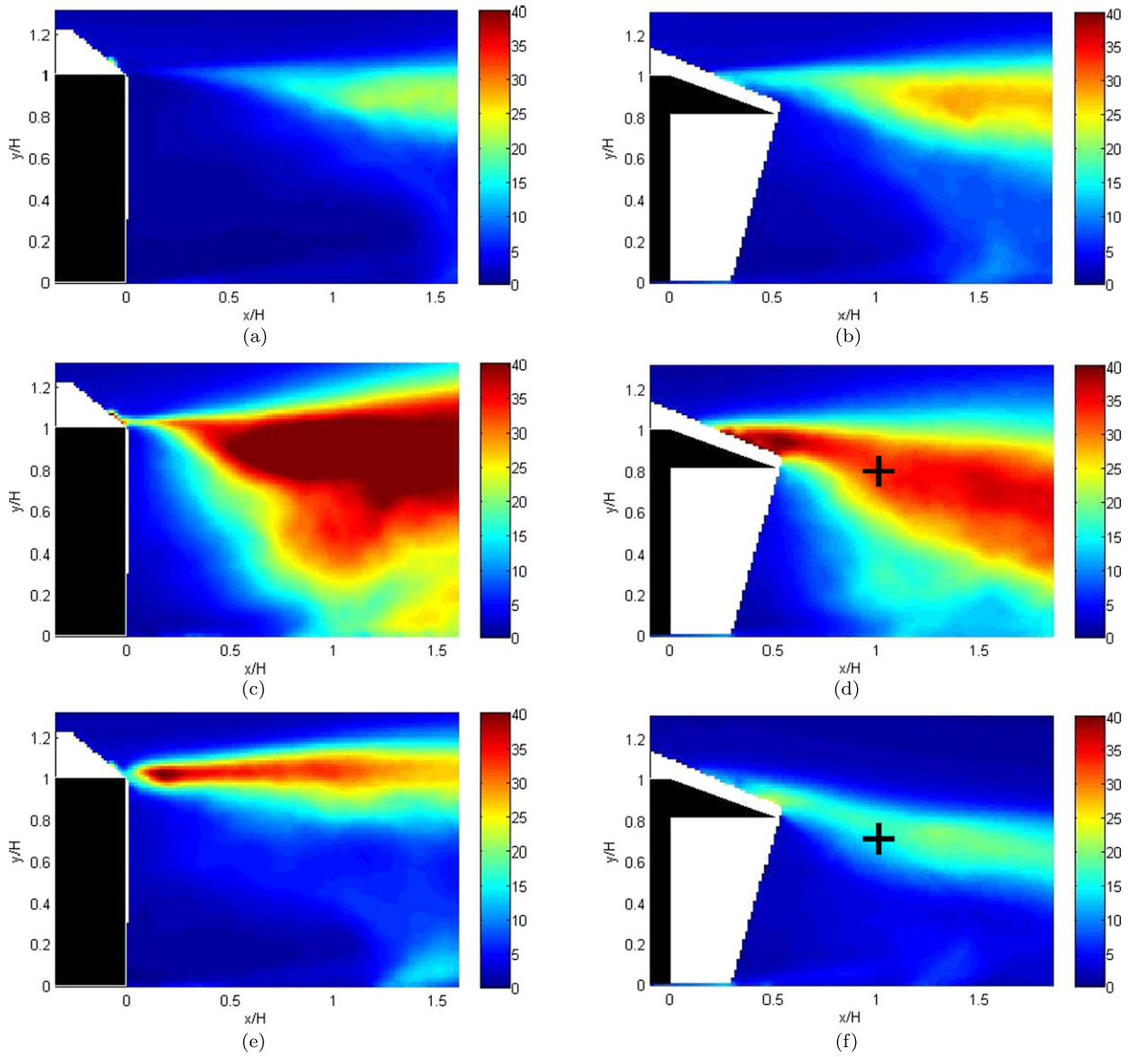

Fig. 4. Velocity fluctuations kinetic energy fields for:
- The square-back configuration with the pulsed jet system off (a), actuated at $St_H = 0.1$ (c) and $St_H = 1.2$ (e);
- The flap configuration with the pulsed jet system off (b), actuated at $St_H = 0.1$ (d) and $St_H = 1.2$ (f).

The origin of the coordinate system is taken at the lower edge of the model rear end. In (d) and (f), the (+) symbols indicate the measurement points used in Fig. 6.

for both square-back and flap configurations. Results are given for two different values of τ; the first one, $\tau_1 = 0$, gives the space-correlation maps and the second one, τ_2, corresponds to a time delay of half an actuation period. The value of τ_2 depends obviously on St_H.

At $\tau = \tau_1$, high correlation values are obtained over a large region in the wake for the low frequency actuation in both configurations, as indicated in Figs. 5(a) and 5(c). These large scale structures in the near-wake are responsible of the minimum value of pressure measured at the rear end of the model. With an actuation Strouhal number St_H of 1.2, the interaction between the incoming flow and the pulsed jet results in a train of small scale vortices. This stream is nearly horizontal in the square-back configuration as depicted in Fig. 5(e) and remains attached to the flap in the flap configuration (Fig. 5(g)). In this configuration, the train of vortices heads down the flap and is then dissipated within the wake. The mean flow remains attached to the flap wall until its trailing edge, thus vectoring the shear layer and narrowing the wake size as observed in Fig. 3(f). This narrower wake size due to the addition of the flap combines with a low velocity fluctuation intensity within the wake to make the rear end pressure increase. The convection velocity U_c of the disturbances induced by the pulsed jet is determined by tracking the spatial location of R_{vv} positive peak values as a function of the time delay τ.

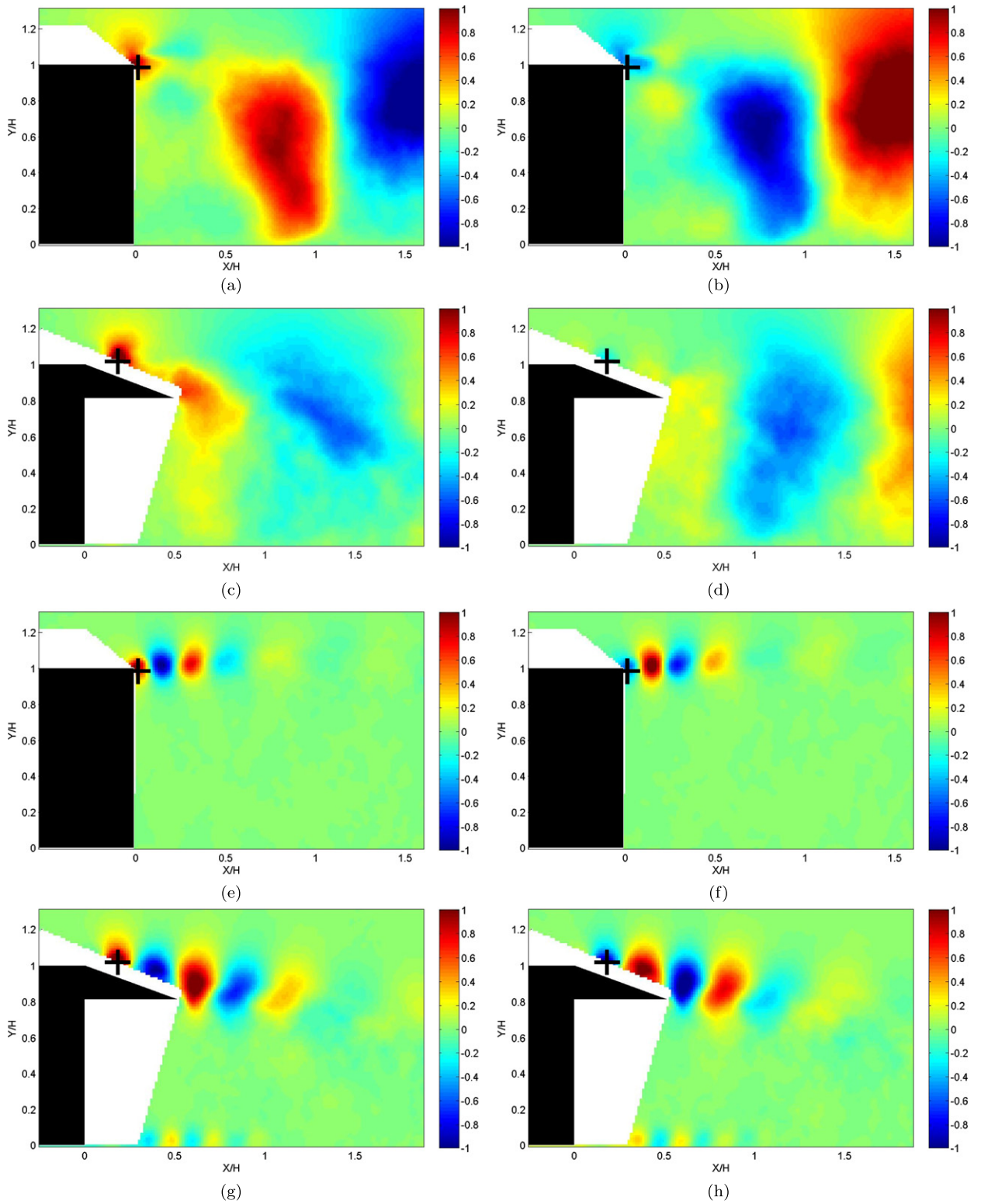

Fig. 5. Maps of the space–time correlation coefficient for:
• Square-back configuration for $St_H = 0.1$ at $\tau_1 = 0$ (a), $\tau_2 = \frac{H}{2U_\infty St_H}$ (b) and for $St_H = 1.2$ and $\tau_1 = 0$ (e), $\tau_2' = \frac{H}{2U_\infty St_H}$ (f);
• Flap configuration for $St_H = 0.1$ at $\tau_1 = 0$ (c), $\tau_2 = \frac{H}{2U_\infty St_H}$ and for $St_H = 1.2$ (d) and $\tau_1 = 0$ (g), $\tau_2' = \frac{H}{2U_\infty St_H}$ (h).
The origin of the coordinate system is taken at the lower edge of the model rear end.

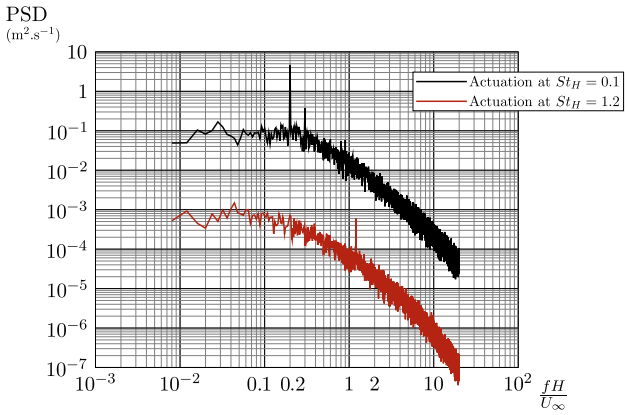

Fig. 6. PSD of velocity measured in the shear layer at the points of maximum E_T indicated in Fig. 4 (——) PSD for $St_H = 0.1$; (——) $10^{-2} \times$ PSD for $St_H = 1.2$ (the 10^{-2} factor is used for clarity reasons).

U_c is found to be nearly equal to $U_\infty/2$, which highlights the fact that the highest rear end pressure recovery is obtained when the characteristic convective time l/U_c is of the same order as the jet actuation period $\frac{H}{U_\infty St_H}$.

The examination of the results obtained with $\tau = \tau_2$ allows to shed some light on the typical frequencies that are observed in the near-wake flow. For the square-back configuration, one remarks in Figs. 5(b) and 5(f) that the high-level correlation patterns compare well with those obtained for $\tau = \tau_1$ but with a spatial shift equal to half the wavelength of the generated disturbance. A similar behaviour is observed for the flap configuration with pulsed jets actuated at $St_H = 1.2$ in Fig. 5(h). This tends to show that the actuation frequency imposes the frequency of the disturbances in the near-wake flow.

In the flap configuration with an actuation Strouhal number St_H of 0.1, as shown in Fig. 5(d), the high-level correlation patterns also compare well with those obtained for $\tau = \tau_1$ in Fig. 5(c). In contrast with previous cases, the sign of each local extremum of the correlation coefficient remains the same as that observed in Fig. 5(c). This suggests that the characteristic frequency of the disturbances in the near-wake flow is, in this case, an harmonic of the actuation frequency. To confirm this, the time evolution of the velocity in the (x, z) plane has been measured in the flap configuration by hot-wire anemometry for the two actuation Strouhal numbers studied. The probe has been located in the shear layer at a distance $X/H = 1$ from the model rear end and at a vertical location corresponding to the maximum of E_T in each case considered as indicated in Figs. 4(d) and 4(f). The resulting power spectral densities are given in Fig. 6 as a function of the Strouhal number based on the model height H. One observes peaks emerging from a broadband level; the frequency of the peaks depends on the actuation Strouhal number. For $St_H = 1.2$, the peak is obtained at the same St_H; for $St_H = 0.1$, peaks are obtained at $2St_H$ and $3St_H$, confirming the harmonic relationship conjectured above. Further investigations are needed to explain this phenomenon.

4. Conclusion

The effects of flow control on the rear end static pressure of a two-dimensional bluff body of height H are studied experimentally for a Reynolds number equal to 1.76×10^5. In particular, the evolution of the mean static pressure coefficient C_p measured at the rear end of the model when varying the actuation frequency is considered. In the square-back configuration, C_p values obtained with flow control are below that of the reference case. A noticeable minimum in C_p is obtained for a St_H around 0.1 which suggests similarities between the flow around the studied geometry and that over a backward-facing step in spite of the underside flow velocity U_u. In the flap configuration, the rear end pressure is slightly below the reference value in a low-frequency range of limited bandwidth, but increases at higher frequencies. Above St_H equal to 0.6, the C_p value is nearly constant and corresponds to a significant drag reduction.

The analysis of the near-wake flow reveals first that, in cases where a pressure increase is obtained, the mean flow is deflected towards the flap wall and thus the recirculation area is reduced. Secondly, space–time correlation maps clearly highlight the periodic features both in time and space of the flow in the near-wake. In both square-back and flap configurations, at low frequencies, the scale of generated vortex structures is of the order of H. On the contrary, small scale vortex structures are generated at high frequencies, which explain well the difference of static pressure measurements in each case. For the flap configuration, hot-wire anemometry measurements show that the frequency of the disturbances in the near-wake is two times the actuation frequency in the low actuation frequency range. Conversely, at higher actuation frequencies, the unsteady feature of the wake flow is dominated by the jet actuation frequency.

Further investigations are planned to correlate the time evolution of C_p with the wake flow properties. Moreover, additional experiments in the control nozzle exit region will help in understanding how the actuation frequency influences the interaction between the pulsed jets and the incoming flow. The detailed study of this interaction could provide information

on the governing mechanisms that lead to static pressure increase at the model rear-base. In the prospect of a closed-loop control, the understanding of these mechanisms may help in choosing the sensors and their locations for efficient control.

Acknowledgements

This work is carried out in the framework of the TIGRE project supported by the Agence pour le développement et la maîtrise de l'énergie (ADEME). We are also grateful to Renault Trucks SAS and LMFA Research teams for their technical support.

References

[1] L.L. Shi, Y.Z. Liu, H.J. Sung, On the wake with and without vortex shedding suppression behind a two-dimensional square cylinder in proximity to a plane wall, J. Wind Eng. Ind. Aerodyn. 98 (2010) 492–503.
[2] K.R. Cooper, The effect of front-edge rounding and rear-edge shaping on the aerodynamic drag of bluff vehicles in ground proximity, Technical Report, SAE Technical Paper, SAE International, 1985.
[3] S. Kowata, J. Ha, S. Yoshioka, T. Kato, Y. Kohama, Drag force reduction of a bluff-body with an underbody slant and rear flaps, Technical Report, SAE Int. J. Commer. Veh., 2008.
[4] S. Li, Analysis of numerical simulation on reducing drag of van body truck, Technical Report, SAE Technical Paper, SAE International, 2011.
[5] A. Brunn, W. Nitsche, Drag reduction of an Ahmed car model by means of active separation control at the rear vehicle slant, in: H.-J. Rath, C. Holze, H.-J. Heinemann, R. Henke, H. Hanlinger (Eds.), New Results in Numerical and Experimental Fluid Mechanics V, in: Notes on Numerical Fluid Mechanics and Multidisciplinary Design, vol. 92, Springer, Berlin, Heidelberg, 2006, pp. 249–256.
[6] C. Leclerc, E. Levallois, A. Kourta, P. Gilliéron, Aerodynamic drag reduction by synthetic jet: A 2d numerical study around a simplified car, Technical Report 2006-3337, in: 3rd AIAA Flow Control Conference, 2006.
[7] J.-C. Béra, M. Michard, M. Sunyach, G. Comte-Bellot, Changing lift and drag by jet oscillation: experiments on a circular cylinder with turbulent separation, Eur. J. Mech. B, Fluids 19 (5) (2000) 575–595.
[8] J. Dandois, E. Garnier, P. Sagaut, Numerical simulation of active separation control by a synthetic jet, J. Fluid Mech. 574 (2007) 25–58.
[9] K.B. Chun, H.J. Sung, Control of turbulent separated flow over a backward-facing step by local forcing, Exp. Fluids 21 (1996) 417–426.
[10] M.A.Z. Hasan, The flow over a backward-facing step under controlled perturbation: laminar separation, J. Fluid Mech. 238 (1992) 73–96.
[11] M. Pastoor, L. Henning, B.R. Noack, R. King, G. Tadmor, Feedback shear layer control for bluff body drag reduction, J. Fluid Mech. 608 (2008) 161–196.
[12] S. Krajnovic, J. Fernandes, Numerical simulation of the flow around a simplified vehicle model with active flow control, Int. J. Heat Fluid Flow 32 (1) (2011) 192–200.
[13] M. El-Alti, P. Kjellgren, L. Davidson, Drag reduction for trucks by active flow control of the wake behind the trailer, in: Proceedings of the Sixth International Symposium on Turbulence, Heat and Mass Transfer, 2009.
[14] D. Krentel, R. Muminovic, A. Brunn, W. Nitsche, R. King, Application of active flow control on generic 3d car models, in: R. King (Ed.), Active Flow Control II, in: Notes on Numerical Fluid Mechanics and Multidisciplinary Design, vol. 108, Springer, Berlin, Heidelberg, 2010, pp. 223–239.
[15] E. Wassen, S. Eichinger, F. Thiele, Simulation of active drag reduction for a square-back vehicle, in: R. King (Ed.), Active Flow Control II, in: Notes on Numerical Fluid Mechanics and Multidisciplinary Design, vol. 108, Springer, Berlin, Heidelberg, 2010, pp. 241–255.